Theoretical and experimental assessment of ion extraction phenomena

IEPC-2019-804

Presented at the 36thInternational Electric Propulsion Conference
University of Vienna • Vienna, Austria
September15-20, 2019

M. Mallon[1], R. Kozakov[2], P. Smirnov[3], M. Smirnova[4], P. Spaedtke[5] and J. Schein[6]
Bundeswehr University Munich, Werner-Heisenberg-Weg 37, Neubiberg, 85577, Germany

and

N. Wallace[7]
ESA ESTEC, Keplerlaan 1, Noordwijk, 2201 AZ, Netherlands

Abstract: The use of high purity xenon remains a significant cost driver against the widespread use of Electric Propulsion technology. In the study reported in this paper options for permissible alternative propellants for a radio frequency ion thruster (RIT) have been selected. This paper describes the development of an overall thruster description, where numerical simulations of the system integrate behavior from the ion source (COMSOL) to the ion optics (Kobra3D). In a first approach xenon and other alternative propellants will be evaluated using computational and experimental methods. To provide improved input for the modeling the densities of all – charged and neutral – species will be determined with high spatial resolution by using spectroscopic as well as probe measurements. Once this has been achieved successfully, the improved modeling shall give us the feasibility to estimate erosive effects on the ion grid system. The modeling of erosive effects is taken out with secondary particle calculations of the Kobra3D code combined with energy deposition calculations using TRIM/SRIM code. Prediction of the geometrical modifications of the ion grid system resulting from the aforementioned energy depositions and of the influence on the ion trajectories can then obtained.

[1]Scientific assistant, LPT, EIT1, michael.mallon@unibw.de
[2]Scientific assistant, LPT, EIT1, ruslan.kozakov@unibw.de
[3]Scientific assistant, LPT, EIT1, pavel.smirnov@unibw.de
[4]Scientific assistant, LPT, EIT1, maria.smirnova@unibw.de
[5]Scientific assistant, LPT, EIT1, peter.spaedtke@unibw.de
[6]Professor, LPT, EIT1, jochen.schein@unibw.de
[7]Electric Propulsion Engineer, TEC-MPE, neil.wallace@esa.int.

Nomenclature

RIT	=	radio frequency ion thruster
OES	=	optical emission spectroscopy
LAAS	=	laser atom absorption spectroscopy
CRM	=	collisional radiative model

I. Introduction

IN the past efforts have been made to replace Xenon by other propellants like Krypton[1] or Iodine[2] as well as to utilize specific mixtures of gases for the particular tasks, e.g. Nitrogen and Oxygen mixture for Air-breathing Electric Propulsion (RAM-EP)[3] or Carbon Dioxide for Mars exploration[4]. In the study presented here, the mixture of Xenon with small amount of Nitrogen is investigated. The focus of the ongoing project lies in the investigation of influence of impurity on grid erosion. Comparison between pure xenon and xenon with admixture shall be made. The numerical model of the plasma; which is used for the prediction of grid erosion needs experimental validation which is the subject of present study.

The spectroscopic diagnostics is often used for the plasma characterization in the electric propulsion engines[6-8].It has advantage of being non-intrusive and in some cases local (e.g. when cylindrical symmetry enables Abel inversion procedure). The disadvantage lies in the non-direct connection between measurable quantities like densities of radiating species and desired plasma parameters like electron temperature and density. In some cases assumptions can be made which enable simple estimation of plasma parameters. For example in the case of thermal equilibrium, the distribution of the excited species densities over the excitation energies should obey Boltzmann law. However sufficient collision frequencies are required to establish Boltzmann distribution. This suggests that both the densities of neutrals and electrons are high enough to allow for this condition. The typical pressure range of RIT operation lies far outside validity of thermal equilibrium. The plasma in both RIT and in its plume is highly non-equilibrium. For the correct estimation of the plasma parameters the model of the excitation and de-excitation of atoms by electrons have to be established. The simplest example of such model is the so called corona model (CM) where excitations are performed by electrons and de-excitations are carried out by radiative decay. The applicability of CM is limited to the regions with small electron densities or to the spectroscopic lines with large transition probabilities. In general case the collisional radiative model have to be established which describes competing processes of radiative and collisional de-excitation of radiating species. This topic is addressed in this paper. Experimental values of the excited species densities are compared with the prediction of the CRM to obtain the relevant plasma parameters.

The paper is structured as follows: first, the experimental set-up is described in section II, followed by the description of the computational modeling in section III, this contains the calculations for the CRM which is used to deduce plasma parameters from the spectroscopic measurements. The results of the measurements and discussion is given in section IV followed by short conclusion and outlook.

II. Experimental set-up

A. Vacuum facility

The vacuum facility consists of two chambers. Main bigger chamber with volume of 4.5 m^3 is pumped by three turbo-molecular pumps and two cryo vacuum pumps. The smaller test chamber (pumped by one turbo-molecular pump) with volume 0.5 m^3 is connected to the main chamber through a gate valve. The rest pressure value of 10^{-6} mbar and $5 \cdot 10^{-8}$ mbar, with and without RIT operation can be reached respectively. The RIT is installed in the test chamber where optical ports enable access for spectroscopic diagnostics.

B. Spectroscopy

The spectroscopic set-up consists of 0.5 m Czerny-Turner spectrograph (SpectraPro HRS-500, Princeton instruments) equipped with a cooled CMOS 2D array detector (AndoriStar-CMOS). The image of the plasma plume is focused onto entrance slit of the spectrograph by 0.2 m achromatic lens. The two mirror periscope system is used to rotate the plasma image axis perpendicularly to the slit orientation. This allowed the radial profile of the radiation intensity to be recorded. Distance between plasma and entrance slit is 1.4 m resulting in spatial resolution of 28 micrometers/pixel.

Spectra in the range between 475 and 925 nm are taken, using 1200 groove/mm grating. This range was scanned by series on recordings each covering 25 nm range. An order sorting filter with 475nm wavelength threshold is used. The spectral resolution is ~0.08 nm full width at half maximum (FWHM). The measurements are calibrated by comparison with the radiometric calibration standard (OL345R, Optronic laboratories).

Example of the spectrum acquired in the region 750-900 nm is shown in Fig.1.Xe lines from transitions between $5p^5 6p$ and $5p^5 6s$ are indicated. Also weak transitions in the $5p^5 6p'$ and $5p^5 6s'$ system can be measured. Vertical scale is expanded by factor 10 in the lower half of the figure to enable better view of the faint lines. The rising noise level in the long wavelength range indicates smaller sensitivity of spectroscopic setup.

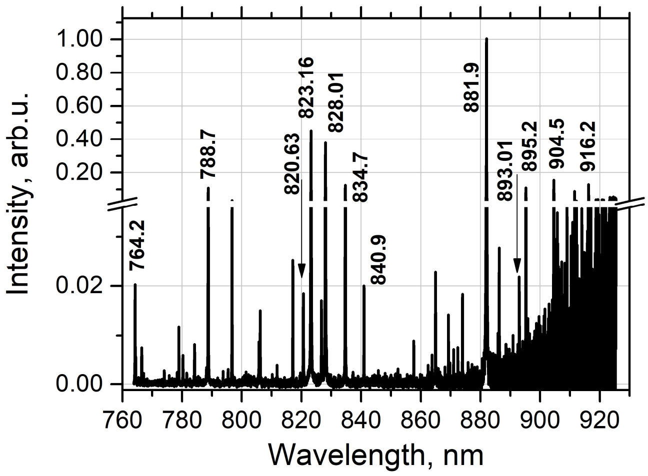

Figure 1. Example of experimental spectrum.

C. Thruster

The RIT-3.5 is used for the investigations. The gas flow rate is set to 1.5 sccm and high purity xenon gas is used (purity 99.999%).

III. Computational modeling

A. Software architecture

The structure outlined in Fig.2 display the essential work flows that need to be addressed in a closed loop physical description of the erosion phenomena of a ion grid in RIT thrusters. The model generates data of the ion source, depending on the electrical circuitry and input parameters to control the source. The interface parameters are then passed to a distinct ion optics simulation, which contains the geometry of the ion grids and ion/ neutral particle densities at the mentioned interface to the ion source.

The data generated from the ion optics code are evaluated using self developed code to extract the information on particle energies and colliding angles with the surrounding metal grid structure. A detailed low dimensional erosion calculation is performed taking into account the four essential mechanisms that arise from the interaction of high energetic ions colliding with matter, which stands in contrast to simpler models like Ref. 5. These are sputtering by ions/ recoil atoms and phonon generation by ions/ recoil atoms. This data is further processed using own developed scripts to derive erosion rates for the regarded material and geometry. The circle in the graphic shall outline that the architecture is designed for temporal evolution of the whole erosion process, with consecutive adaption of the ion grid geometry and the corresponding impact on the ion beams.

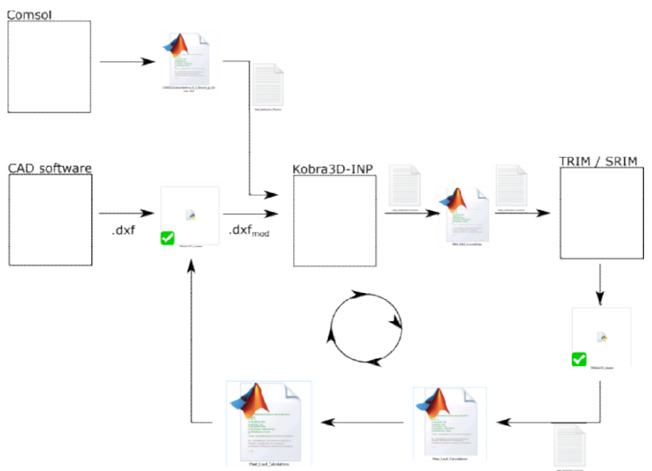

Figure 2. Software architecture for the integrated development environment. Taking into account the dynamics of ion source, ion optics, erosion modeling and heat transport within the ion grids.

B. Reactions and Cross-sections

Following electron-heavy particle collisions are considered in the plasma chemistry model:

$$e^- + Xe \rightarrow Xe^* + e^- \quad (1)$$

$$e^- + Xe^m \leftrightarrow Xe^* + e^- \quad (2)$$

$$e^- + Xe^m \leftrightarrow Xe^r + e^- \quad (3)$$

$$Xe + Xe^m \leftrightarrow Xe + Xe^r \quad (4)$$

$$e^- + Xe \rightarrow Xe^+ + 2e^- \quad (5)$$

$$e^- + Xe^* \leftrightarrow Xe^+ + 2e^- \quad (6)$$

with the superscript m indicating metastable states, and superscript r indicating resonant states.

The cross-sections for direct excitations (1) are taken from Ref. 9. The stepwise excitation (2) cross-sections are calculated according to Ref. 10 and modified according to the note in Ref.11 for better coincidence with the values measured in Ref 12. The intermixing constant for reactions (3) and (4) is taken from Ref 13 and 14 respectively. The reactions (3) and (4) are considered only for $5p^56s$ and $5p^56s'$ level systems exclusively, i.e. there is no intermixing between those two systems. The reactions (5) and (6) account for direct ionization and indirect ionization from excited state, they are derived from Ref.10.

The excitation rates are calculated for Maxwellian electron energy distribution function. The rates of stepwise de-excitation are obtained from the detailed balance considerations and direct excitation rates. The value of the reduced electron mobility of xenon is derived from Ref.15.

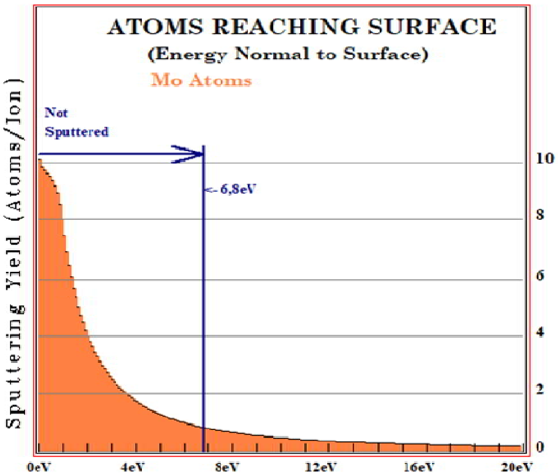

Figure 3. Spatial resolved sputtering rate of molybdenum atoms by incident xenon particles at zero degree angle and at energies of 1keV.

C. Collisional Radiative Model: System of Equations

For the collisional processes described by Eq. (1)-(4) following system can be written in steady state case:

$$M \cdot \vec{N} = \vec{D}$$

Where $\vec{N}$ the vector of unknown densities of is excited species, $\vec{D}$ is the vector of direct excitations rates and M is the so called relaxation matrix. Vector $\vec{N}$ consists of 14 elements representing 4 excited levels $5p^56s$ and 10 excited levels $5p^56p$. Elements of vector $\vec{D}$ are written as

$$D_i = N_e N_0 \langle v\sigma_{0i} \rangle,$$

Where N_0 is the density of Xenon in ground state, N_e is the electron density, $\sigma_{0i}$is the direct excitation cross-section[9]. Brackets represent average of the cross-section over the Maxwellian distribution function.

Diagonal elements of matrix M represent depopulation rates of excited levels by escape of resonant radiation and stepwise excitation (levels s2 and s4 in Paschen notation); diffusion to the plasma edge and stepwise excitation (levels s4 and s5); and radiative decay and stepwise de-excitation for $5p^56p$ levels. Non-diagonal elements of M represent populating processes from other considered levels to the current level either by radiative or stepwise processes.

For the first four equations which describe the $5p^56s$ levels, additional terms of intermixing processes between metastable and radiating levels [Eq. (3)-(4)] appear both in diagonal and off-diagonal elements of M.

D. Ion source and ion optics modeling

The ion source is modeled with the use of COMSOL Multiphysics software version 5.4. It is built upon the geometry of a simple inductive coupled plasma source, the boundary conditions for the set up are: the inlet mass flow rate 1.5 sccm, input rf power 30W, reference pressure level 25 Pa. The model delivers the particle and current densities at the interface towards the ion optics. For experimental purposes the model delivers the plasma potential within the ion source and the particle density of the excited xenon atoms at the outlet. To ease the comparability of the computational results to the measurements the

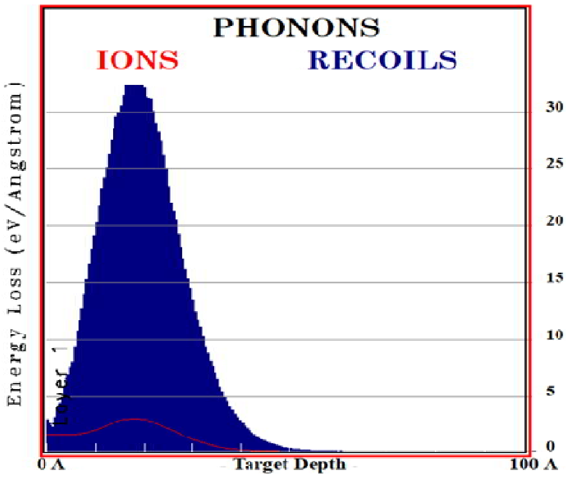

Figure 4. Spatial resolved phonon generation rate within the molybdenum target by inciding xenon particles at zero degree angle and at energies of 1keV.

density of excited atoms is expanded into the volume of the ion optics since the Langmuir probe measurements are taken around 20 mm distant from the ion source interface. The expansion is conducted after a simplified formula, derived for the case of expansion into vacuum without geometrical boundaries. This will be adapted further on with the integration of a more detailed molecular dynamics simulation of the neutral particle movement within the ion optics.

The ion optics calculations are conducted using Kobra3D-INP software, which can solve the trajectories of primary particles for 2 dimensional and 3 dimensional ion grid structures. Furthermore Kobra3D-INP delivers data on the generation rate of secondary ions created in the volume of the ion optics due to CEX collisions with the background neutral particles, as mentioned above this will be modified using a more detailed molecular dynamics model.

E. Erosion modeling

The information on particle trajectories delivered by the ion optics code is now the baseline for the erosion calculations. First the range on particle energies and incident angles towards the metal surfaces of the grids is deduced. These are input parameters for the particle in matter ranging calculations, which are processed using the TRIM/SRIM code, briefly described in Ref. 16. Currently the geometry of the ion grid is simplified to a one dimensional surface; the target material is defined as a monolayer target of a characteristic length, which is defined by thermal simulations. The TRIM/SRIM code generates the differential and integral sputtering rates for each boundary condition, which can be used to model the geometry change due to sputtering phenomena. Furthermore the generation rate of induced phonons is delivered, which is a differential quantity for the collective vibrations within a crystalline structure. In pure metals this can be directly connected to the heat dissipation in a first approximation. These phonons contribute to the generation of heat in a very thin layer of the metal grid, depending on the number of incident ions and are typically in the order of a few Angstrom. The impact of this heat source on the evaporation of metal particles close to the surface, as well as movement of the particles within the crystalline structure cannot be disregarded and require more detailed analysis on the temporal evolution of the heat within the ion grid. This is best carried out by switching the perspective to a quantum mechanical model which accounts better for the dynamics of phonons within the metal structure. A heat transport simulation for this one dimensional structure is added with the distribution of phonons as input parameters, the total length of the molybdenum layer was therefore extended to 1 mm.

IV. Results and Discussion

The measurement of absolute intensity of spectroscopic lines enables direct calculation of the densities of excited species, if transition probabilities are known. We restrict ourselves therefore to the spectroscopic region between 760 and 916 nm where suitable lines can be measured. Example of the evaluation of is shown in Fig.5. Densities of the excited xenon atoms in the configuration $5p^5 6p$ can be measured, except of level p10 (Paschen notation) whose transitions lies outside sensitivity region of our measurement system. For levels which have two spectroscopic lines the doubled symbols at given level give estimation of measurement accuracy. The absolute value of densities and their distribution over the excitation levels can be compared with the results of CRM model for Te=6 eV, Ne=10^{15} m^{-3} and neutral gas pressure 10^{-3} mbar, which are shown in Fig.6. The plasma parameters were chosen to obtain best possible coincidence between the model and the measurement. In general model still delivers higher than measured values of excited species densities. Especially for the case of p1-p4 levels the discrepancy can reach factor 30. The best coincidence is reached for level p8 which delivers only factor 2.5 discrepancy.

The Fig. 3 and 4 show the differential sputtering and phonon distributions for a 1000 Angstrom molybdenum monolayer target. The result of a one dimensional heat transport simulation shows a significant heating within the first 100 Angstrom of the target material. The temperature induced by this mechanism exceeds the melting and evaporation temperature molybdenum. Some critical points can be derived from this estimation, a higher dimensional simulation need to be carried out to ensure the number of incident particles was not tremendously overestimated. Furthermore with a spatial resolved model the temperature distribution lateral to the metal surface can be analyzed, this would account for important heat sinks that have been disregarded in the one dimensional simulation, but would certainly lower the overall temperature of the metal close to the surface. If the just mentioned points can be eliminated as source of uncertainty, one has to consider the detailed quantum dynamical behavior of the phonons to further analyze the phenomenon. The approximation that phonons and heat transport are directly coupled only truly holds if the structure of the crystal is somewhat homogenous and the scattering of phonons on crystal defects can be neglected. Taking these effects into account would change the heat capacity and thermal conductivity of the metal in the proximity of the region where the phonons are induced by the incident ions. This would again alter the distribution of the heat within the metal and might reduce the temperature significantly. At last this phenomenon can also be resolved by taking evaporation of metal atoms close to the surface into account. This would be a new source of erosion of the metal structure. Based on the current data, the impact of this phenomenon will be further analyzed to evaluate its importance compared to sputtering phenomena.

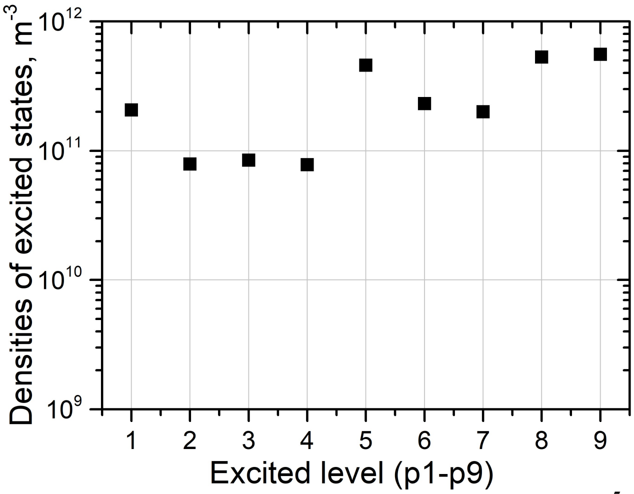

Figure 5. Experimental values of the densities in the 5p^{5}6p system. Represented are measured p1 to p9 levels in Paschen notation.

V. Conclusion and Outlook

Results of the first measurements in the plasma plume of the RIT are presented. The CRM for the plasma is described. Comparison of the model outcomes and experimental measurements indicate that the model should be modified to obtain smaller discrepancy. This can be achieved by inclusion of other excited levels in the model, especially 5p^{5}5d, 5p^{5}7s and 5p^{5}7p levels whose excitation energies are comparable with 5p^{5}6p levels and whose spectroscopic lines are available for evaluation.

No absorption signal could be detected in the plasma plume after single pass of the laser beam. The improvement of the LAAS diagnostics with lock-in detection scheme will be performed to achieve sensitivity increase.

On the computational modeling side the displayed framework shall give us the feasibility to estimate erosive effects on the ion grid system. Some crucial steps need to be undertaken to ensure the reliability of the generated data. First the intersections to physical parameters that are visible to experimental methods need to be extended. Most interesting here would be method to derive measurements of the temperature evolution in the ion grids. Furthermore missing links in the interconnects of each distinct software need to be resolved to ensured that errors emerging from the software can be localized and limited on their impact on the overall uncertainty of the results. A constantly evolving sensitivity analysis of the system errors is part of the development of that framework. Numerical convergence is currently not guaranteed for all operational parameters only specific sets of operational conditions have been taken as inputs so far. The physics of phonon dynamics and heat transfer within the metal lattice need to be further analyzed. As well as the physics behind the intersecting topics of structural „weakening" due to vacancy generation by ion impact and the propagation of phonons in metal grids need to be derived. The simplified assumption of neutral particle density evolution within the ion optics volume must be enhanced with a micro scale particle dynamics simulation.

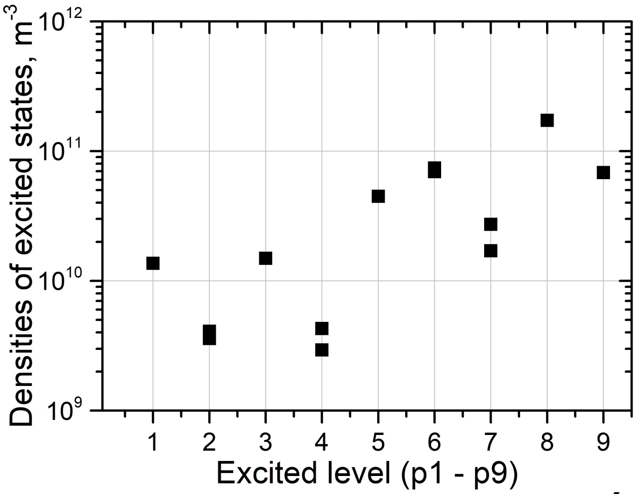

Figure 6. Calculated values of the densities in the 5p^{5}6p system

Acknowledgments

The project was supported by ESA contract 4000124912/18/NL/KML

References

[1]Patterson, M. and Williams, G., "Krypton Ion Thruster Performance," NASA TM-105818, 1992.

[2]Szabo, J., Robin, M., Paintal, S.,Pote, B., Hruby, V. and Freeman, C., "Iodine Propellant Space Propulsion," *International Electric Propulsion Conference*, Washington, DC, 2013, IEPC-2013-311

[3]Cifali, G.,Misuri, T., Rossetti, P.,Andrenucci, M., Valentian, D., Feili, D. and Lotz, B., "Experimental

characterization of HET and RIT with atmospheric propellants," *International Electric Propulsion Conference*, Wiesbaden, Germany, 2011, IEPC-2011-224

[4]Hohman, K., "Atmospheric breathing electric thruster for planetary exploration," *NIAC spring symposium*, Pasadena, CA, 2012

[5]Wirz, R. E., Anderson, J. R., Katz, I.,"Time-Dependent Erosion of Ion Optics," *Journal of Propulsion and Power*, Vol. 27, No. 1., January-February 2011, DOI: https://doi.org/10.2514/1.46845

[6]Chiu, Y., Austin, B.L., Williams, S., Dressler, R.A. and Karabadzhak G.F., "Passive Optical Diagnostics of Xe-propelled Hall Thrusters. I. Emission Cross Section," *J. Appl. Phys.*, Vol. 99, 2006, 113304.

[7]Karabadzhak G.F., Chiu, Y., and Dressler, R.A., "Passive Optical Diagnostics of Xe-propelled Hall Thrusters. II. Collisional-Radiative Model," *J. Appl. Phys.*, Vol. 99, 2006, 113305.

[8]Yang J., Yokota, S., Kaneko, R. and Komurasaki, K., "Diagnosing on Plasma Plume from Xenon Hall Thruster with Collisional-Radiative Model," *Phys.Plasmas*, Vol. 17, 2010, 103504.

[9]Allan, M., Zatsarinny, O., and Bartschat, K., "Near-threshold absolute angle-differential cross sections for electron-impact excitation of argon and xenon" *Phys. Rev. A*,Vol. 74,2006, 030701 (R).

[10]Vriens L., and Smeets, A. H. M., "Cross-section and rate formulas for electron-impact ionization, excitation, deexcitation, and total depopulation of excited atoms" *Phys. Rev. A*, Vol. 22, 1980, pp. 940-951.

[11]Gortchakov,S., Lange, H. and Uhrlandt, D., "Model of a He-Xe low pressure dc positive column plasma" *J. Appl. Phys.*, Vol. 93, 2003, pp. 9508-9515.

[12]Jung, R.O., Boffard, J.B., Anderson, L.W. and Lin, C.C.., "Electron-impact excitation cross sections from the xenon J=2 metastable level" *Phys. Rev. A*, Vol. 72, 2005, 022723.

[13]Ivanov, V. A., Makasjuk, J.V., Prikhodko, A.S. and Skoblo, Y.E., "Rate constants for deactivation of He(2^1S_0), Ar($4s^3P_2$), Xe($6s^3P_2$) by electrons in plasma," *ESCAMPIG*, Orleans, France, 1990, pp. 94-95

[14]Wieme, W., "Decay of excited species in the afterglow of a pulsed discharge in xenon," *J. Phys. B.:Atom.Molec.Phys*, Vol. 7, 1974, pp.850-856.

[15]Bordage, M. C., Biagi, S. F., Alves, L. L., Bartschat, K., Chowdhury, S., Pitchford, L. C. Hagelaar, G. J. M., Morgan, W. L., Puech, V. and Zatsarinny, O., "Comparisons of sets of electron–neutral scattering cross sections and swarm parameters in noble gases: III. Krypton and xenon," *J. Phys. D.:Appl. Phys.*, Vol. 46, 2013, 334003

[16]*Ziegler,J.F.,(2004).* "SRIM-2003". Nucl. Instrum. Methods Phys. Res. B. *219-220: 1027.* Bibcode:2004NIMPB.219.1027Z. doi:10.1016/j.nimb.2004.01.208.